



**ESA MesosphEO**

**MesosphEO WP 3.6**  
**ATBDs for merging algorithms, products and error**  
**characterisation**

Michael Kiefer, KIT  
Stefan Lossow, KIT

FMI-TN-MesosphEO-WP3-006  
Version 1.3  
Tuesday 12<sup>th</sup> December, 2017 21:01 CET



## Contents

<b>1</b>	<b>Preamble</b>	<b>3</b>
<b>2</b>	<b>De-seasonalisation</b>	<b>3</b>
<b>3</b>	<b>Merging</b>	<b>4</b>
<b>4</b>	<b>Limited validation</b>	<b>5</b>
4.1	Comparison parameters . . . . .	5
4.2	Results for water vapour . . . . .	7
4.3	Results for temperature . . . . .	9
<b>5</b>	<b>Version history</b>	<b>15</b>



## 1 Preamble

Based on the considerations and discussions in WP 3.2 we focus on the time series merging of de-seasonalised water vapour and temperature data, to avoid the irreconcilable differences in the annual variation among the individual data sets. As input monthly zonal mean (using  $10^\circ$  bins) time series are used, preferably those produced in WP 4.3. In the following section we describe the de-seasonalisation. In Sect. 3 the merging approach is detailed and in Sect. 4 results from a limited validation of the merged data are presented.

## 2 De-seasonalisation

De-seasonalisation can be achieved in multiple ways. A common approach is to calculate for a given calendar month the average over several years. Subsequently this average is subtracted from the individual months contributing to the average. This approach requires that a data set covers every calendar month at least twice. The MIPAS data sets obtained with full spectral resolution from July 2002 to March 2004 do not fulfil this criterion. To keep these data sets as a part of the merging we use instead a regression approach for the de-seasonalisation. Every data set is regressed with following regression model:

$$f(t, \phi, z) = C_{\text{offset}}(\phi, z) + C_{\text{AO}_1}(\phi, z) \cdot \sin(2 \cdot \pi \cdot t/p_{\text{AO}}) + C_{\text{AO}_2}(\phi, z) \cdot \cos(2 \cdot \pi \cdot t/p_{\text{AO}}) + C_{\text{SAO}_1}(\phi, z) \cdot \sin(2 \cdot \pi \cdot t/p_{\text{SAO}}) + C_{\text{SAO}_2}(\phi, z) \cdot \cos(2 \cdot \pi \cdot t/p_{\text{SAO}}). \quad (1)$$

The model contains an offset, the annual (AO) and the semi-annual (SAO) variation. The AO and SAO are parametrised by orthogonal sine and cosine functions. In the equation  $t$  denotes the time in years,  $f(t, \phi, z)$  the fit of the time series for a given latitude band  $\phi$  and altitude  $z$  and  $C$  are the regression coefficients of the individual model components.  $p_{\text{AO}}=1$  year is the period of the annual variation, likewise  $p_{\text{SAO}}=0.5$  year is the period of the semi-annual variation. To calculate the regression coefficients we follow the method outlined by *von Clarmann et al.* [2010] using the standard errors  $\epsilon(t, \phi, z)$  (their inverse squared) of the monthly zonal means as statistical weights. Autocorrelation effects and empirical errors [Stiller et al., 2012] were not considered in the regression. The de-seasonalised time series  $y_d(t, \phi, z)$  are then given as:

$$y_d(t, \phi, z) = y(t, \phi, z) - f(t, \phi, z), \quad (2)$$

with  $y(t, \phi, z)$  denoting the non-de-seasonalised (or absolute) data. For the sake of simplicity we do not assign any error to the regression fit, so that  $\epsilon_d(t, \phi, z) = \epsilon(t, \phi, z)$ .



### 3 Merging

To merge the individual data sets at a given time  $t$  (i.e. monthly mean) we calculate a weighted average:

$$y_m(t, \phi, z) = \frac{\sum_{i=1}^{n(t, \phi, z)} w_i(t, \phi, z) \cdot y_{d_i}(t, \phi, z)}{\sum_{i=1}^{n(t, \phi, z)} w_i(t, \phi, z)} \quad (3)$$

where  $w_i(t, \phi, z)$  is the weighting of the individual data sets and  $n(t, \phi, z)$  describes the total number of data sets to be merged. Implicitly, all parameters depend on latitude band and altitude. The weighting of the individual data sets is calculated as follows:

$$w_i(t, \phi, z) = \frac{1}{\epsilon_{d_i}(t, \phi, z)^2 + s(z)^2} \quad (4)$$

The weighting is based on two terms, i.e. the standard error of the monthly zonal means and a typical spread  $s$  among the data sets. The former term characterises a combination of noise error and natural variability. The spread term is intended to characterise systematic uncertainties of the individual data sets. In an ideal situation dedicated analyses of the systematic uncertainties would exist for all data sets. Since this is, however, not the case we choose a different approach to characterise the systematic uncertainties. For that we combine the data of all data sets. At a given time and latitude band we derive the spread (i.e. the maximum difference) among all de-seasonalised data sets. Prior to this determination we screen the data to avoid outliers and consequently overly large and unrealistic spread estimates. The screening is based on the median and the median absolute difference (MAD) [Jones *et al.*, 2012]. Data points outside the range  $\{\text{median}[y_d(t, \phi, z)] \pm 7.5 \cdot \text{MAD}[y_d(t, \phi, z)]\}$  are discarded. For the merging we have tested weightings with the described latitude- and time-dependent spreads. However, any such separation does not matter much for the final result. In correspondence, we use a single spread profile, derived as the average over the spreads derived for all monthly means and latitude bands.



The combined error of the merged data set is given as follows:

$$\epsilon_m(t, \phi, z) = \frac{1}{W(t, \phi, z)} \cdot \sqrt{\sum_{i=1}^{n(t, \phi, z)} w_i(t, \phi, z)^2 \cdot \epsilon_{d_i}(t, \phi, z)^2} \quad \text{with} \quad (5)$$

$$W(t, \phi, z) = \sum_{i=1}^{n(t, \phi, z)} w_i(t, \phi, z).$$

This equation assumes that there no covariances between the individual data sets.

We merge the time series derived from the complete data sets. In addition there are also attempts to merge the time series separated according to daytime and nighttime. This, however, limits the number of available data sets, as the solar occultation measurements by ACE-FTS or SCIAMACHY are performed in twilight conditions and thus do not allow a meaningful separation according to the time of day. Likewise the solar scatter observations by OSIRIS and SCIAMACHY cover primarily daytime.

The merged de-seasonalised time series are provided in NetCDF files. A detailed description of those is provided in WP 4.4.

## 4 Limited validation

For the merged data sets a limited validation has been performed. In this section we describe the comparison parameters that were considered and show the results for water vapour and temperature.

### 4.1 Comparison parameters

We concentrate on three parameters for the validation. The first one is the bias  $b(t, \phi, z)$  between the merged de-seasonalised time series  $y_m(t, \phi, z)$  and the comparison time series  $y_{\text{comp}}(t, \phi, z)$ :

$$b(t, \phi, z) = y_m(t, \phi, z) - y_{\text{comp}}(t, \phi, z). \quad (6)$$

Besides that, we calculate the correlation coefficient  $r(t, \phi, z)$  between the merged and comparison time series, to evaluate how well the temporal variability matches in these



data sets:

$$r(\phi, z) = \frac{\sum_{i=1}^{n_t(\phi, z)} [y_m(t_i, \phi, z) - \overline{y_m}(\phi, z)] \cdot [y_{\text{comp}}(t_i, \phi, z) - \overline{y_{\text{comp}}}(\phi, z)]}{\sqrt{\sum_{i=1}^{n_t(\phi, z)} [y_m(t_i, \phi, z) - \overline{y_m}(\phi, z)]^2} \cdot \sqrt{\sum_{i=1}^{n_t(\phi, z)} [y_{\text{comp}}(t_i, \phi, z) - \overline{y_{\text{comp}}}(\phi, z)]^2}} \quad (7)$$

with

$$\overline{y_m}(\phi, z) = \frac{1}{n_t(\phi, z)} \cdot \sum_{i=1}^{n_t(\phi, z)} y_m(t_i, \phi, z) \quad \text{and} \quad (8)$$

$$\overline{y_{\text{comp}}}(\phi, z) = \frac{1}{n_t(\phi, z)} \cdot \sum_{i=1}^{n_t(\phi, z)} y_{\text{comp}}(t_i, \phi, z) \quad (9)$$

where  $n_t(\phi, z)$  describes the number of monthly means available for comparison at a given latitude and altitude.

Finally we determine the drift over time between the merged and the comparison data set. For that we regress the bias  $b(t, \phi, z)$  with a regression model that contains an offset, a linear term which describes the drift, the annual and semi-annual variation as well as variation caused by the QBO:

$$\begin{aligned} f(t, \phi, z) = & C_{\text{offset}}(\phi, z) + C_{\text{linear}}(\phi, z) \cdot t + \\ & C_{\text{AO}_1}(\phi, z) \cdot \sin(2 \cdot \pi \cdot t/p_{\text{AO}}) + C_{\text{AO}_2}(\phi, z) \cdot \cos(2 \cdot \pi \cdot t/p_{\text{AO}}) + \\ & C_{\text{SAO}_1}(\phi, z) \cdot \sin(2 \cdot \pi \cdot t/p_{\text{SAO}}) + C_{\text{SAO}_2}(\phi, z) \cdot \cos(2 \cdot \pi \cdot t/p_{\text{SAO}}) + \\ & C_{\text{QBO}_1}(\phi, z) \cdot \text{QBO}_1(t) + C_{\text{QBO}_2}(\phi, z) \cdot \text{QBO}_2(t). \end{aligned} \quad (10)$$

In the regression model the QBO variation is described by proxies in the form of normalised winds at 50 hPa (QBO<sub>1</sub>) and 30 hPa (QBO<sub>2</sub>) over Singapore (1°N / 104°E). The winds at these two pressure levels are approximately orthogonal [e.g. *Stiller et al.*, 2012]. The information on the Singapore winds is provided by the Free University in Berlin (<http://www.geo.fu-berlin.de/met/ag/strat/produkte/qbo/qbo.dat>). For the calculation of the regression coefficients we follow again the method outlined by *von Clarmann et al.* [2010]. As statistical weights we use the inverse squared of the combined error of the bias  $\epsilon_b(t, \phi, z)$ , i.e.:

$$\epsilon_b(t, \phi, z) = \sqrt{\epsilon_m(t, \phi, z)^2 + \epsilon_{\text{comp}}(t, \phi, z)^2}. \quad (11)$$



Unlike for the de-seasonalisation of the individual data sets, autocorrelation effects and empirical errors [Stiller *et al.*, 2012] are considered in the drift determination to derive optimal uncertainty estimates of this quantity.

## 4.2 Results for water vapour

To validate the merged data set for water vapour we use observation of the MLS (Microwave Limb Sounder, Waters *et al.*, 2006) instrument aboard the Aura satellite. The instrument provides data since August 2004 and observations are still ongoing. Correspondingly the validation period spans from 2004 to 2017. The Aura satellite uses a sun-synchronous orbit yielding a latitude coverage from about 82°S to 82°N. Water vapour observations are performed daily and information can be retrieved up to about 85 km. In this comparison MLS results derived with the retrieval version 4.2 are considered [Livesey *et al.*, 2015]. The principal vertical coordinate of the MLS data is pressure. Geometric altitudes are derived from the simultaneous observation of temperature, in combination with a start height taken from a climatology.

Figure 1 shows the bias between the merged de-seasonalised time series and the MLS time series for the latitude band between 50°N and 60°N. The bias is typically within  $\pm 0.4$  ppmv, which is in range of the typical uncertainty in the observations [e.g. Nedoluha *et al.*, 2009; Nedoluha *et al.*, 2017]. The lowest deviations occur on average in the lowermost stratosphere. There are occasionally obvious fluctuations between positive and negative biases on short time scales. Likewise there are at times rather large biases, like in early 2015 or around the turn from 2016 to 2017.

In Figure 2 the correlation coefficients between the merged de-seasonalised time series and the MLS time series are shown. In most cases the correlation coefficients exceed values of 0.5. The largest correlation coefficients are observed in the lowermost stratosphere. Towards higher altitudes the correlation coefficients slowly decrease. There is no pronounced latitude dependence. For example in the Arctic both rather high and rather low values are observed at different altitudes. Minima in the averaged correlation coefficient over all altitudes are found for the latitude band between 90°S and 80°S and in the northern tropics. Overall, the correlation coefficients are rather large compared to results obtained in other comparisons [Khosrawi *et al.*, in preparation].

Figure 3 shows the drift between the merged de-seasonalised time series and the MLS time series. There is overall a tendency towards negative drifts. Positive drifts are primarily found at low latitudes. Some of those are also statistically significant at the  $2\sigma$  uncertainty level, indicated by the hexagrams in the figure. The largest negative trends are found in the polar latitudes, again occasionally statistically significant. Clearly in the mid-latitudes the best agreement in the long-term behaviour between the merged de-seasonalised time series and the MLS time series is found.

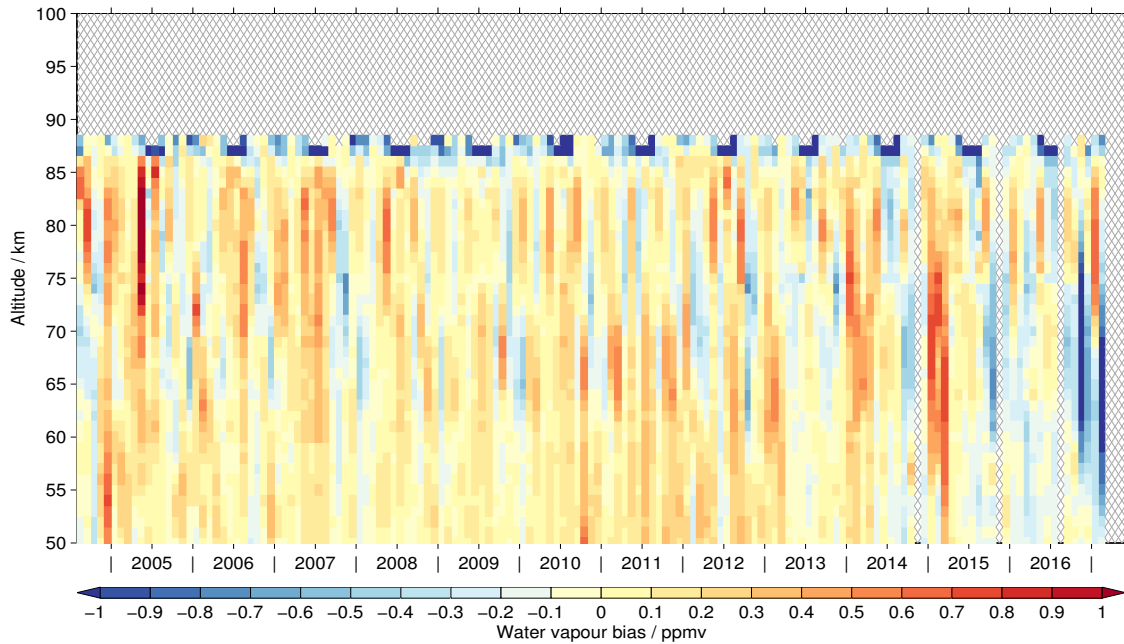


Figure 1: The bias between the merged de-seasonalised time series and the MLS time series. This example considers the latitude band between  $50^{\circ}\text{N}$  and  $60^{\circ}\text{N}$ . White areas with x-marks indicate that there is no overlap between the data sets.

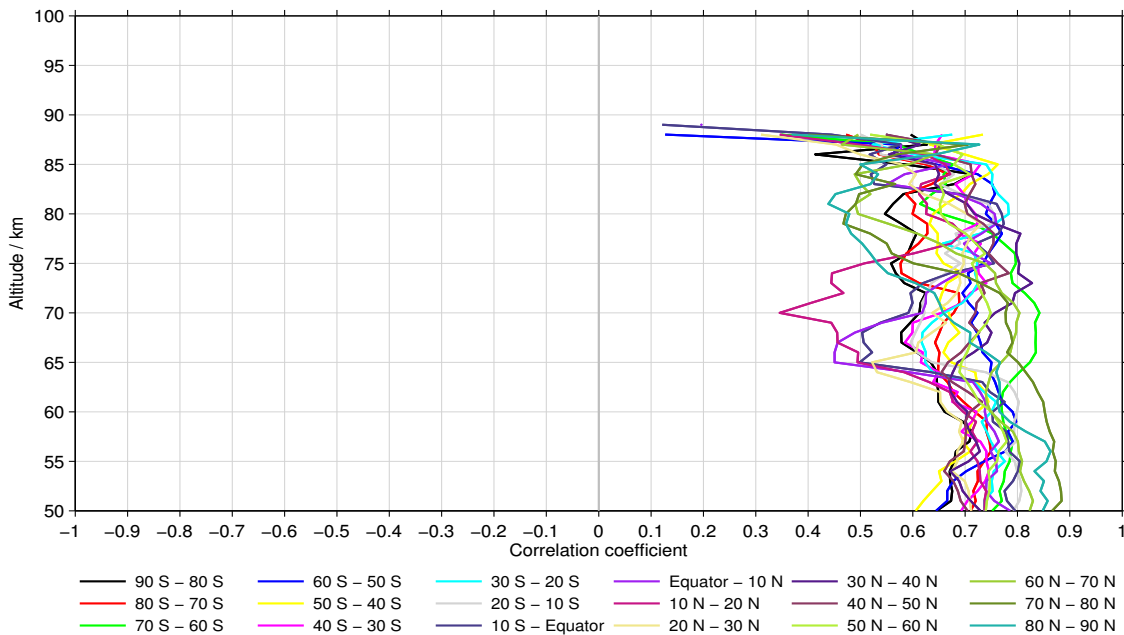


Figure 2: The correlation coefficients between the merged de-seasonalised time series and the MLS time series for different latitude bands.

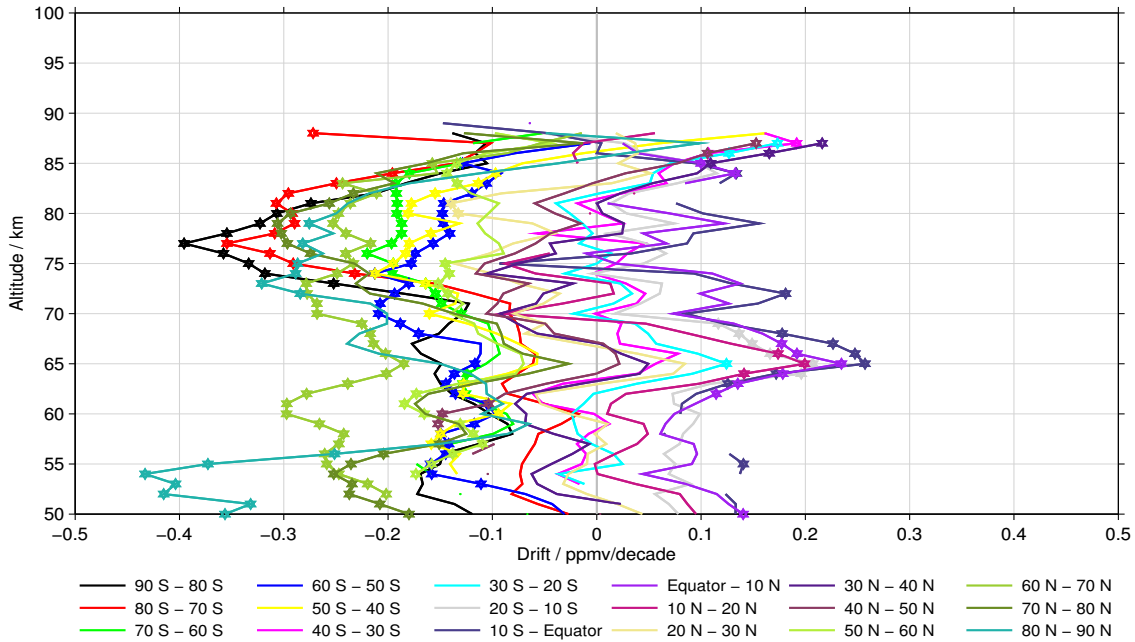


Figure 3: The drift between the merged de-seasonalised time series and the MLS time series. Hexagrams are used to indicate where the drift is significant at the  $2\sigma$  level.

### 4.3 Results for temperature

For temperature two kinds of data sets were generated: The first kind is based on de-seasonalized data sets, while the second consists of original full temperature data. Apart from the different basis for the merged data sets, all calculation steps, either for data generation or validation, are equal between both.

To validate the merged temperature data sets two corresponding reference data sets were generated from MLS 4.2 temperature data. Details for the MLS data can be found in Sect.4.2 as well as a literature reference.

Figure 4 gives two examples of the bias between the deseasonalized merged time series and the corresponding de-seasonalised MLS time series. Here the bias is defined as merged time series minus MLS time series, i.e. a positive bias means that the value of merged time series is greater than the corresponding MLS value. As it is nicely illustrated in the two figure panels the bias depends on the latitude band considered. While for mid-latitude and equatorial latitudes the overall bias often is below  $\pm 1$  K the latitudes polewards of  $60^\circ$ S and  $60^\circ$ N show greater positive and negative deviations of up to 10 K.

Figure 5 shows an example of the bias between the merged time series (i.e. original, not deseasonalized data) and the corresponding MLS time series for the latitude band between  $40^\circ$ S and  $30^\circ$ S. The bias shown illustrates that there is a quite strong discrepancy

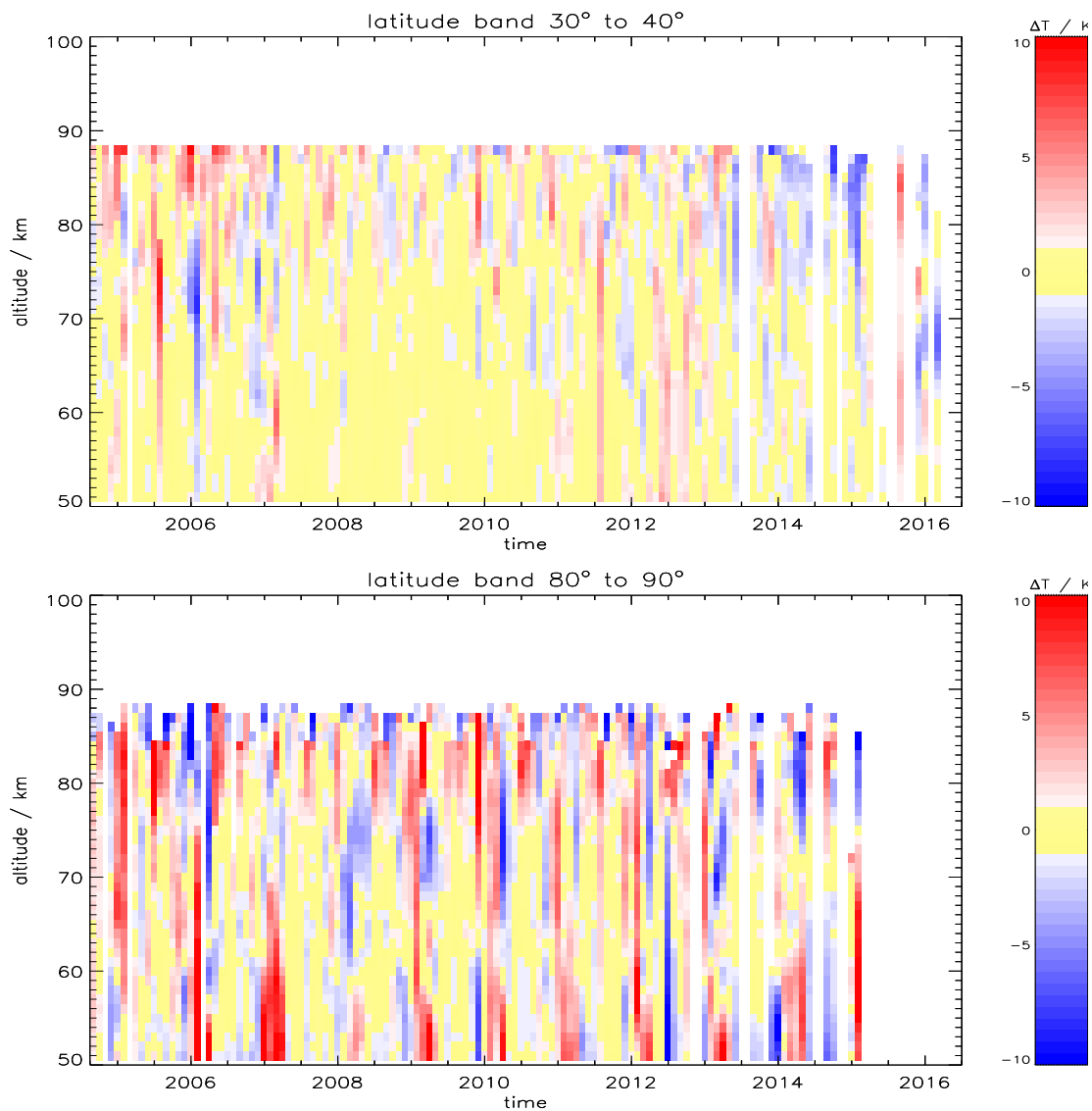


Figure 4: Bias between the merged de-seasonalised time series and the de-seasonalised MLS time series for temperature. These examples consider the latitude band between 30°N and 40°N (upper panel) and between 80°N and 90°N (lower panel). White areas indicate that there is no overlap between the data sets.

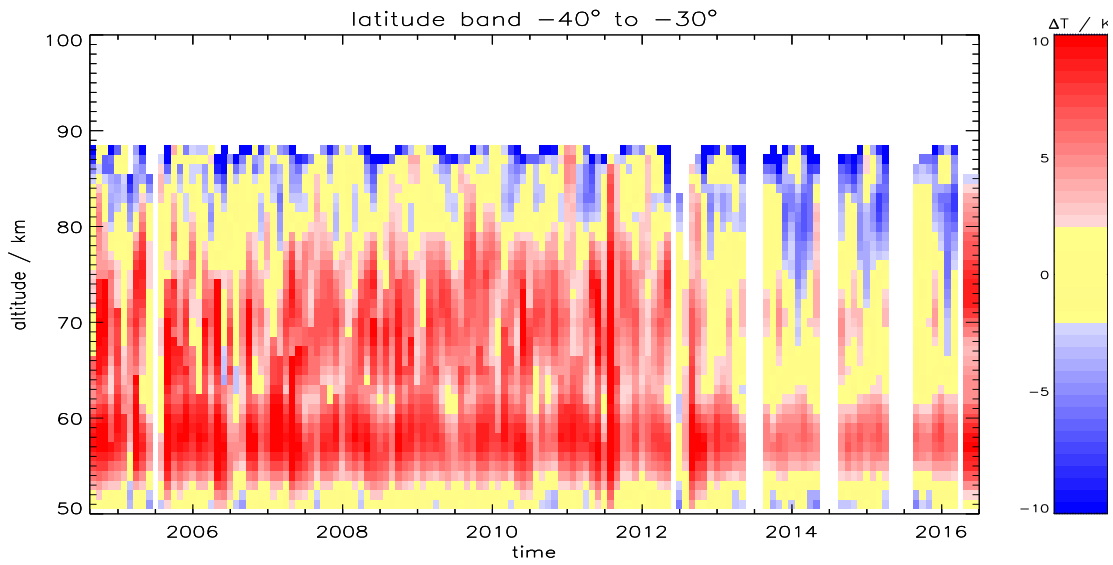


Figure 5: Bias between the merged time series and the MLS time series for temperature. This example considers the latitude band between 40°S and 30°S.

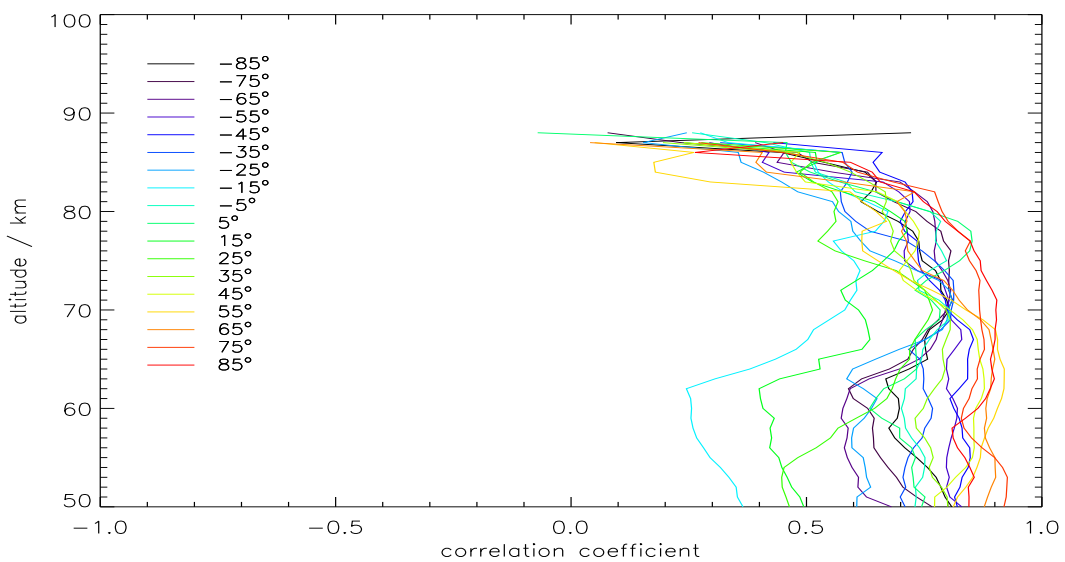


Figure 6: Correlation coefficients between the merged de-seasonalised time series and the de-seasonalised MLS time series for different latitude bands.

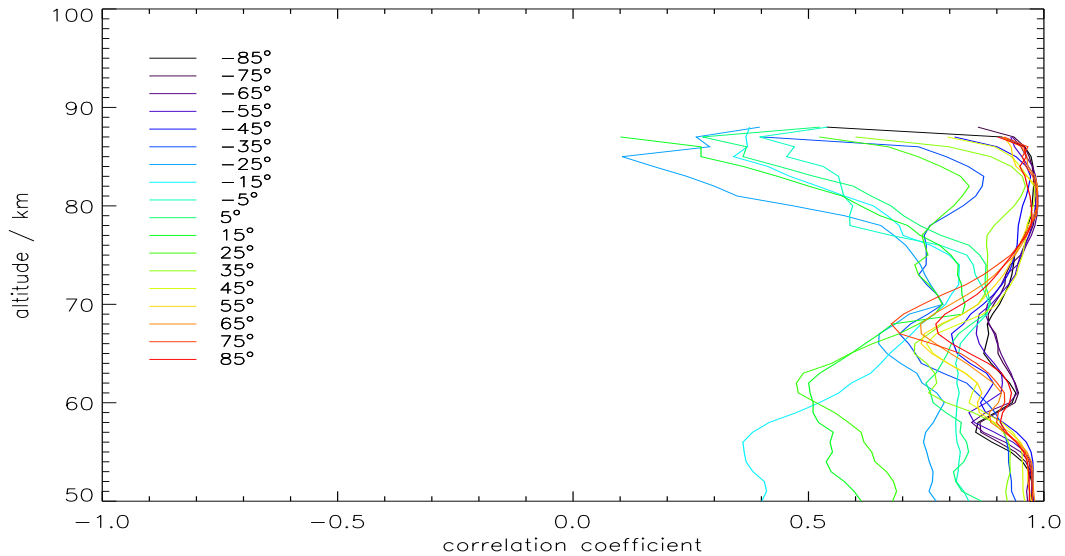


Figure 7: Correlation coefficients between the merged time series and the MLS time series for different latitude bands.

between the merged and the MLS data with positive values of the bias clearly dominating. However, again there is a dependence on the latitude: The bias in the polar regions is only moderately large with a bias amplitude of up to 5 K, rather low in the equatorial region with values in the range of  $\pm 3$  K, and highest in the mid-latitudes, where the amplitudes of the bias reach 10 K. Overall there is a positive bias, mostly concentrated in two altitude bands around 57 and 70 km. The bias in the 70 km band disappears approx. after the begin of 2012 in all latitude bands, indicating that the datasets used only up to this time are the main contributors to this deviation.

In Figure 6 the correlation coefficients between the merged de-seasonalised time series and the corresponding MLS time series is shown. Below 70 km northern latitudes show a higher correlation than southern latitudes and both are better correlated than the equatorial regions. Above 70 km all but few equatorial bands reach approx. the same values, which are, however, rapidly decreasing towards the top of the altitude range.

Figure 7 shows the correlation coefficients between the merged time series and the corresponding MLS time series (both not deseasonalized). This data set exhibits a strong separation between equatorial and low mid latitude and the other latitude bands. The former show much lower values below 65 and above 75 km. Around 70 km there is an increase for the equatorial correlation and a drop in the correlation of the other latitudes.

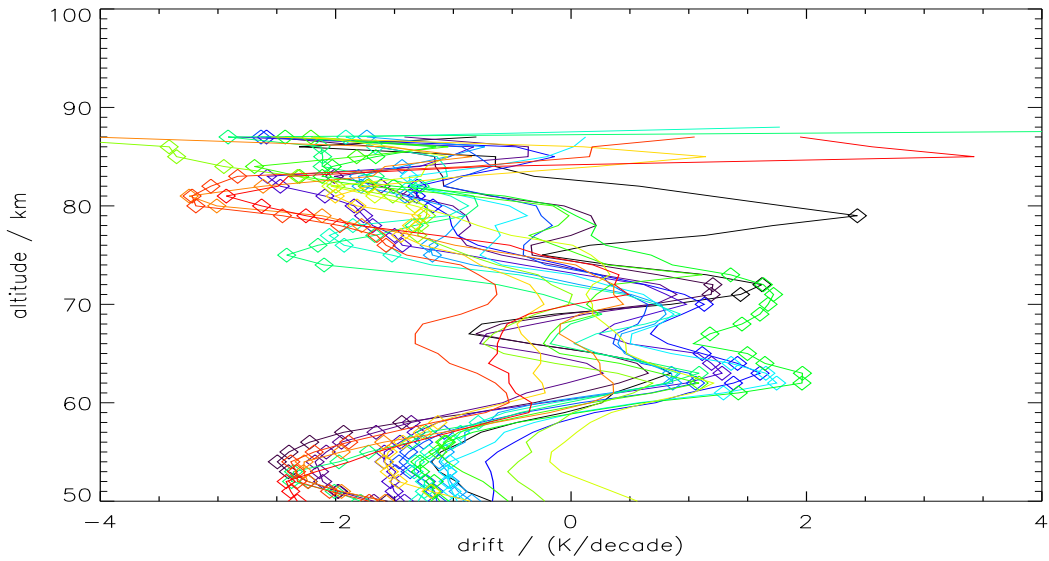


Figure 8: Drift between the merged de-seasonalised time series and the de-seasonalised MLS time series. Diamonds indicate significance at  $2\sigma$  level. Latitude color as in Fig.6.

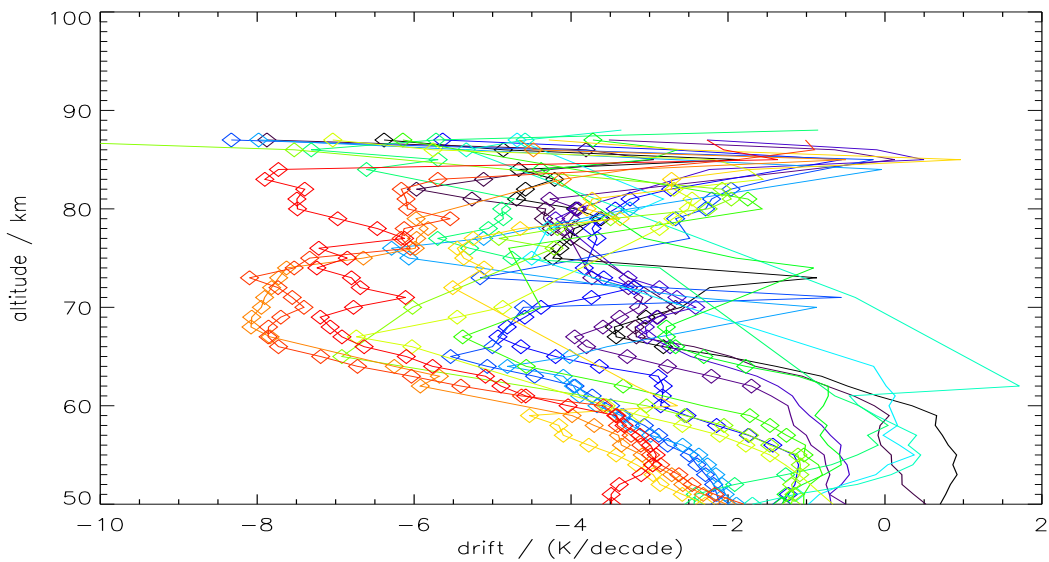


Figure 9: Drift between the merged time series and the MLS time series. Diamonds indicate significance at the  $2\sigma$  level. Color coding of the latitude band as in Fig.6.



Figure 8 shows the drift between the merged de-seasonalised time series and the corresponding MLS time series. A clear separation into three altitude bands is discernible, virtually for all latitudes: Below 58 km almost all latitude bands exhibit a negative drift wrt MLS, the majority even is significant at the  $2\sigma$  level. Between 62 and 73 km there is a band with non-significant drift values around zero for most latitude bands. However, for southern polar to mid-latitudes a significant positive drift is indicated. The third altitude band begins at 74 km. Above this level, and extending to the top of the data set, most latitude bands show negative drifts, which are often significant. It is not clear why there is this formation of three layers with distinct drift behaviour. The data sets which enter the merged product do not have altitude range restrictions compatible with the jump altitudes of the drift.

As depicted in Fig.9 the drift between the merged time series and MLS (both not deseasonalized) essentially is negative with most latitudes reaching significant values throughout the entire altitude range. Exceptions are the southernmost and the southern equatorial latitude bands.

Apart from this general picture the detailed course of the drifts with altitude is complex: Northern high latitude bands show a pronounced step in the drift at altitudes of about 60 km. The values increase from approx. 3 K/decade below to about 7 K/decade above. This behaviour can be well understood from the bias itself. As discussed above the positive bias is strongly reduced after 2012, this will lead to a negative trend in the data set and hence to a negative drift wrt MLS. In general the high values can be considered as an indication that the merged time series of not deseasonalized data might be of no great use.



## 5 Version history

version 1.0 / 17 August 2017

- the initial version

version 1.1 / 30 September 2017

- consideration of the comments by Alexei Rozanov, University of Bremen

version 1.2 / 23 November 2017

- update: results of limited validation added for temperature

version 1.3 / 12 December 2017

- small bugfixes



## References

- Jones, A., et al., Technical Note: A trace gas climatology derived from the Atmospheric Chemistry Experiment Fourier Transform Spectrometer (ACE-FTS) data set, *Atmospheric Chemistry & Physics*, *12*, 5207 – 5220, doi:10.5194/acp-12-5207-2012, 2012.
- Khosrawi, F., S. Lossow, G. Stiller, and J. Urban, The SPARC water vapour assessment II: comparison of stratospheric and lower mesospheric water vapour time series observed from satellites, in preparation.
- Livesey, N. J., et al., Aura/MLS version 4.2x level 2 data quality and description document, [http://mls.jpl.nasa.gov/data/v4-2\\_data\\_quality\\_document.pdf](http://mls.jpl.nasa.gov/data/v4-2_data_quality_document.pdf), last access: 18 August 2017, 2015.
- Nedoluha, G. E., R. M. Gomez, B. C. Hicks, J. E. Wrotny, C. Boone, and A. Lambert, Water vapor measurements in the mesosphere from Mauna Loa over solar cycle 23, *Journal of Geophysical Research*, *114* (D13), D23,303, doi:10.1029/2009JD012504, 2009.
- Nedoluha, G. E., et al., The SPARC water vapor assessment II: intercomparison of satellite and ground-based microwave measurements, *Atmospheric Chemistry and Physics Discussions*, *2017*, 1 – 32, doi:10.5194/acp-2017-578, 2017.
- Stiller, G. P., et al., Observed temporal evolution of global mean age of stratospheric air for the 2002 to 2010 period, *Atmospheric Chemistry & Physics*, *12*, 3311 – 3331, doi:10.5194/acp-12-3311-2012, 2012.
- von Clarmann, T., G. Stiller, U. Grabowski, E. Eckert, and J. Orphal, Technical note: Trend estimation from irregularly sampled, correlated data, *Atmospheric Chemistry & Physics*, *10*, 6737 – 6747, 2010.
- Waters, J. W., et al., The Earth Observing System Microwave Limb Sounder (EOS MLS) on the Aura Satellite, *IEEE Transactions on Geoscience and Remote Sensing*, *44*, 1075 – 1092, doi:10.1109/TGRS.2006.873771, 2006.